ELSEVIER

Nuclear Engineering and Design 177 (1997) 303–319

Nuclear Engineering and Design

On the constitutive description of the Microinteractions concept in steam explosions

X. Chen, W.W. Yuen, T.G. Theofanous *

Center for Risk Studies and Safety, University of California, Santa Barbara, CA 93106, USA

Received 23 December 1996

Abstract

This paper elaborates on the constitutive description of the 'Microinteractions' model used by the computer code ESPROSE.m to simulate the propagation phase of steam explosions. The approach is based on a series of experiments, in the SIGMA-2000 facility, involving molten drops of tin caused to explode under sustained pressure fields, an environment similar to that of a fully developed large-scale detonation. The experimental ranges cover shock pressures of up to 204 bar and melt temperatures of up to 1800°C; a series of isothermal runs, using gallium drops, are also included. The results indicate that, to a first approximation, the basic form of the constitutive laws hypothesized in the original formulation of ESPROSE.m is appropriate. Moreover, through detailed comparison of data with numerical experiments, certain parameters appearing in these laws could be identified quantitatively.

1. Introduction

The purpose of this paper is to follow up on the 'Microinteractions' idea proposed only recently as *the* fundamental ingredient of steam explosion physics (Yuen and Theofanous, 1994). The idea owes its origin to the recognition that in fully developed large-scale detonations, melt fragmentation occurs under a sustained pressure field (as opposed to the sharp-pulse triggers employed in all previous fragmentation studies), and on the observation that under such conditions the debris (fragmented fuel mass) mixes with the coolant found only in the immediate vicinity of the melt–coolant interface (Yuen et al., 1994). The rest of the coolant simply does not participate in the ensuing thermal interaction (but it does participate in the wave dynamics process), and the effect on the feedback obtained is enormous—it can produce sustained detonations under much less restrictive conditions on fuel concentration and fragmentation rates.

The first formulation (Yuen and Theofanous, 1994) of the Microinteractions model was based on the hypothesized constitutive law that the rate of coolant mixing with the debris is proportional to the melt fragmentation rate. This model produced the first, and still only (see, for example, the review by Fletcher and Anderson (1990) that explains the inconsistencies) consistent comparisons with available experimental results (in the KRO-

* Corresponding author. Tel.: +1 805 8934900; fax: +1 805 8934927.

0029-5493/97/$17.00
PII S0029-5493(97)00138-6

Fig. 1. The SIGMA-2000 facility.

TOS facility): from 'weak propagations' with tin melt at 1000°C to supercritical detonations with aluminum oxide melt at 2300°C. This model was also utilized to obtain the first results for two-dimensional detonations (open pool geometries), thus demonstrating the important mitigating effect of 'venting' due to wave reflection at the free pool surface (Theofanous and Yuen, 1994).

In this paper, we examine this constitutive formulation in light of the experiments carried out in the SIGMA-2000 facility especially for this purpose. We use ESPROSE.m to help with the interpretation and in the process we are able to examine the whole Microinteractions model of ESPROSE.m in some detail, as well as certain wave dynamics features of the code.

In this first systematic experimental evaluation of the Microinteractions 'laws', we concentrate on molten tin drops at temperatures up to 1800°C, and shock pressures from 68 to 204 bars (1000–3000 psi). As a basis of comparison, we also carry out a set of experiments under isothermal conditions with gallium drops (melting point at 30°C). The results are used to show the existence of a hydrodynamic regime at high pressures, and of a thermally affected regime at the low end of the pressures considered. Any material dependence is yet to be determined as we undertake experimentation, one-by-one, with each material of interest (namely, Fe and ZrO_2 for reactor applications). However, it is reasonable to expect that, to the extent that the hydrodynamic regime is adequately characterized by the relevant properties (as described below), the behavior at this limit can be predicted adequately. This is *the* important regime from the point of view of assessing the energetics of large-scale detonations. At low pressures, thermal effects set in, but this is relevant to the triggering and early escalation stages of an explosion. Preliminary experiments with iron melts at pressure of 68 bar and 1600°C indicates a thermal effect much stronger than that of tin. This is not surprising considering the heat capacities per unit volume (ρc_p) of iron as compared to that of tin (twice as big). The latent heat of iron is also much larger than that of tin (4 times bigger). To fully understand this regime, we need extensive experiments with various melts and pressures

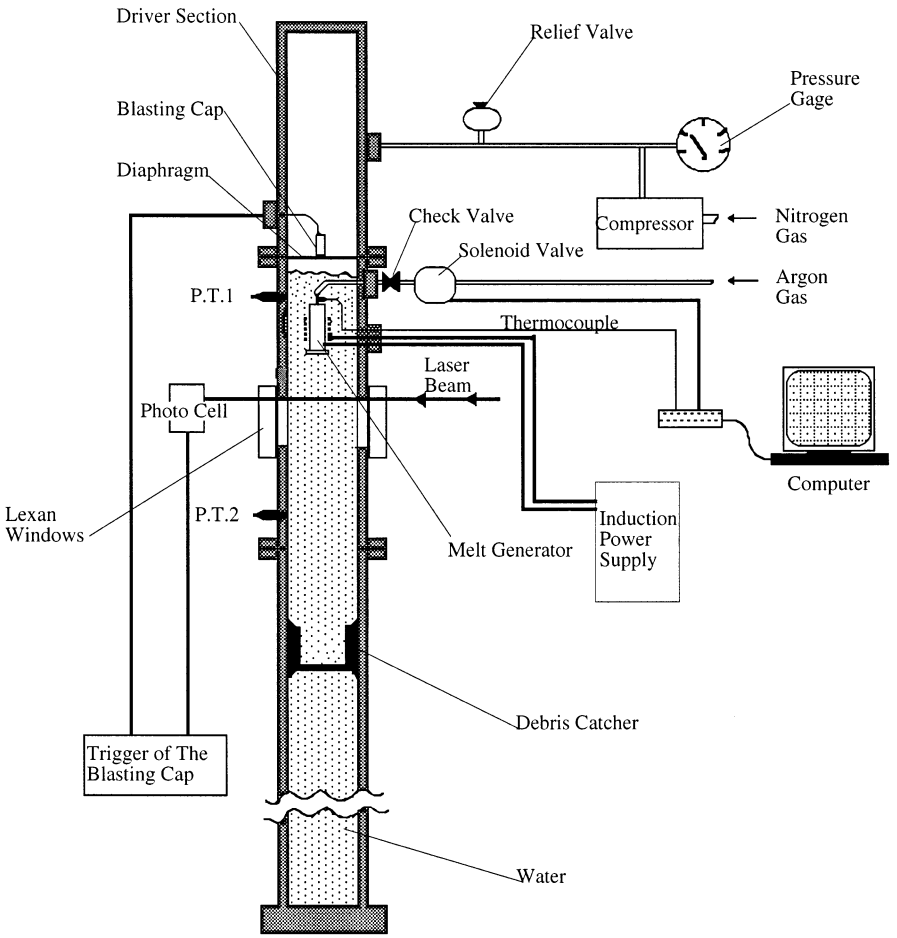

Fig. 2. Schematic of the SIGMA-2000 facility (not to scale).

from essentially ambient up to the range considered here. However, exploring this regime is a lower priority concern, and we are treating it as such.

2. Experimental apparatus and instrumentation

The experiments are carried out in the SIGMA facility, employed previously for the study of fragmentation of mercury drops in water (Patel and Theofanous, 1981) under sustained pressure waves and isothermal conditions. More recently, SIGMA was employed in the study of molten tin drops at temperatures up to 1000°C (Yuen et al., 1994). For the present study, the facility was upgraded to allow melt drop temperatures up to about 2000 K (hence the SIGMA-2000 name). The whole experimental arrangement is shown in Fig. 1, and it can be explained with the help of the schematics in Figs. 2 and 3.

The basic component is the shock tube, consisting of a 1-m-long driver section and a 2-m-long expansion section. The design pressure is 1000 bar, and with water in the expansion section, it allows steady flows/pressures for up to about 2.3 ms, before the reflected wave from the bottom end of the tube arrives back at the window area. The

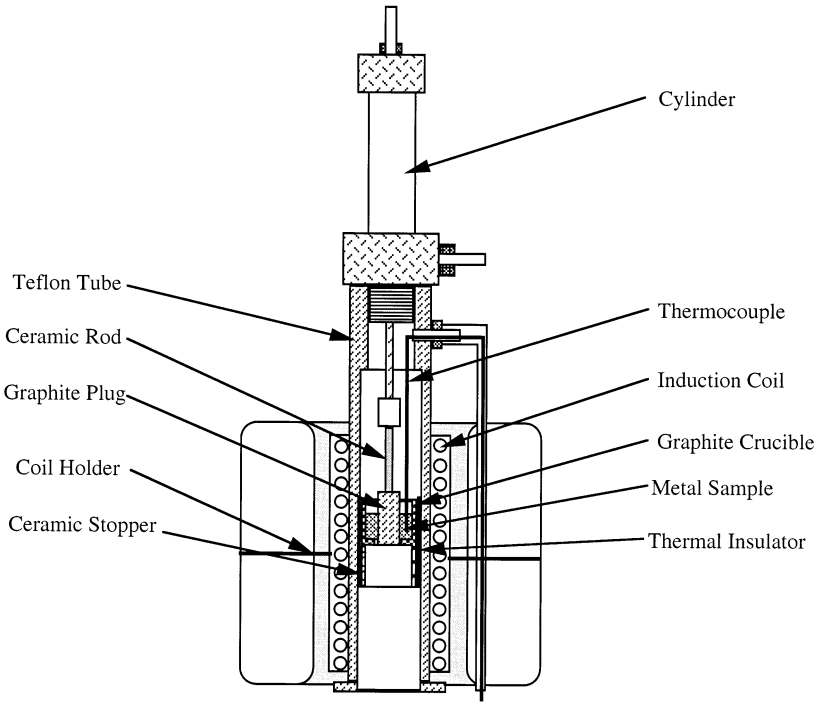

Fig. 3. Schematic of the melt drop generator.

window allows an observation area of 2×5 cm, and its midpoint is located 50 cm below the top of the expansion section, which is separated from the expansion section by a prescored steel diaphragm. The shock wave is initiated by cracking the diaphragm with the help of a blasting cap which is electrically detonated.

The melt generator, typically placed 5 cm above the window, is illustrated in Fig. 3. It is designed to melt and reproducibly release single drops of melt at any desired temperature up to 2073 K (1800°C). The test material is placed inside a graphite crucible, surrounded by an induction coil, powered by a 2.5 kW generator. The sample, and to some degree the crucible, can be heated rapidly by the induction currents while the temperature there is monitored on-line using K-type thermocouples. When the drop temperature reaches the desired value (typical heating time is about 1 min), a mini-plug cylinder (driven by argon gas pressure) is made to snap open, thus releasing a single molten drop. Since at 1300°C the thermocouple fails, higher temperatures are obtained by an on-line fit and extrapolation of the temperature data (using a PC). The procedure is estimated to have an uncertainty of about ± 30°C.

The most challenging aspect of the experiment is to obtain the drop-shock interaction near the top of the observation window, so that the event can be observed in its entirety (as the drop translates rapidly and explodes behind the shock). This is achieved by automatically timing the whole experimental sequence, starting with the detection of the molten drop, by means of a laser beam, at the very top end of the window.

The principal experimental data are images of the exploding drops obtained with flash X-ray and high-speed movies. (So far, these data have been obtained in separate experiments, but under well-reproducible conditions; however, we

Table 1
Test conditions for the SIGMA-2000 experiments

Run ID	Melt	Temperature (melt/water) (°C)	Shock pressure (bar)	Initial drop diameter (horizontal/vertical) (cm)
G/68/45	Gallium	45/45	68	0.68/0.46
G/204/45	Gallium	45/45	204	0.81/0.39
G/272/45	Gallium	45/45	272	0.91/0.56
T/68/1700	Tin	1700/90	68	0.65/0.46
T/204/1800	Tin	1800/90	204	0.63/0.43
T/68/1000	Tin	1000/90	68	0.75/0.41
T/204/1000	Tin	1000/90	204	0.63/0.38

Table 2
Properties of materials

Material	Density (gm cm^{-3})	Surface tension (dyne cm^{-1})	Specific heat (J $(g \cdot K)^{-1}$)	Heat of fusion (J g^{-1})
Gallium	6.07	660	0.371	79.7
Tin	6.10 ($T = 1700$°C); 6.47 ($T = 1000$°C)	550	0.220	60.7
Iron	7.87	1550	0.449	247

have recently developed the capability of simultaneous operation). For the X-ray, we use a Hewlett Packard generator (Model 43734A) capable of a single 25 ns duration flash, that can be timed very precisely on the basis of the shock arrival time at the window. For the movie, we use a rotating drum camera, run typically at 25 000 frames s^{-1}, for a total recording time of 6 ms, under backlighting conditions.

Pressures are measured both above and below the window with flush-mounted quartz piezoelectric transducers (KISTLER, 607L) having a rise time of 1.5 μs and a 30 000 psi maximum range. The signal from the top transducer is used to trigger the X-ray and/or the flash-light for the movie camera. Both transducer signals are recorded in a four-channel digital storage oscilloscope (LeCroy 9304, 175 MHz) and a PC.

Finally, as shown in Fig. 2, we employed a debris catcher (which was able to slide up and down the tube following the flow) to collect the debris after each run, both for mass and debris size distribution analysis.

3. Experimental program and data reduction techniques

Critical aspects for the quantitative radiography employed here are the optimization of the X-ray energy level and source position from the object, such as to optimize the film exposure. Moreover, strict quality standards need to be applied in the reproducible development of the exposed film, detailed calibration curves, and witness pieces on every film, to allow for the small correction always necessary due to intangible variations in the exposure–development–reading process. With these techniques properly established, one can obtain the two-dimensional projection of the fragmenting drop mass distribution at the instant of the X-ray flash. As a means of checking the accuracy of the whole process, the total drop mass was reproducible from the X-ray analysis, typically within 10–15%

The high-speed movies provide the evolution of images of the outside envelope of the Microinteractions region (consisting of the debris, entrained water, and any steam produced by the interaction),

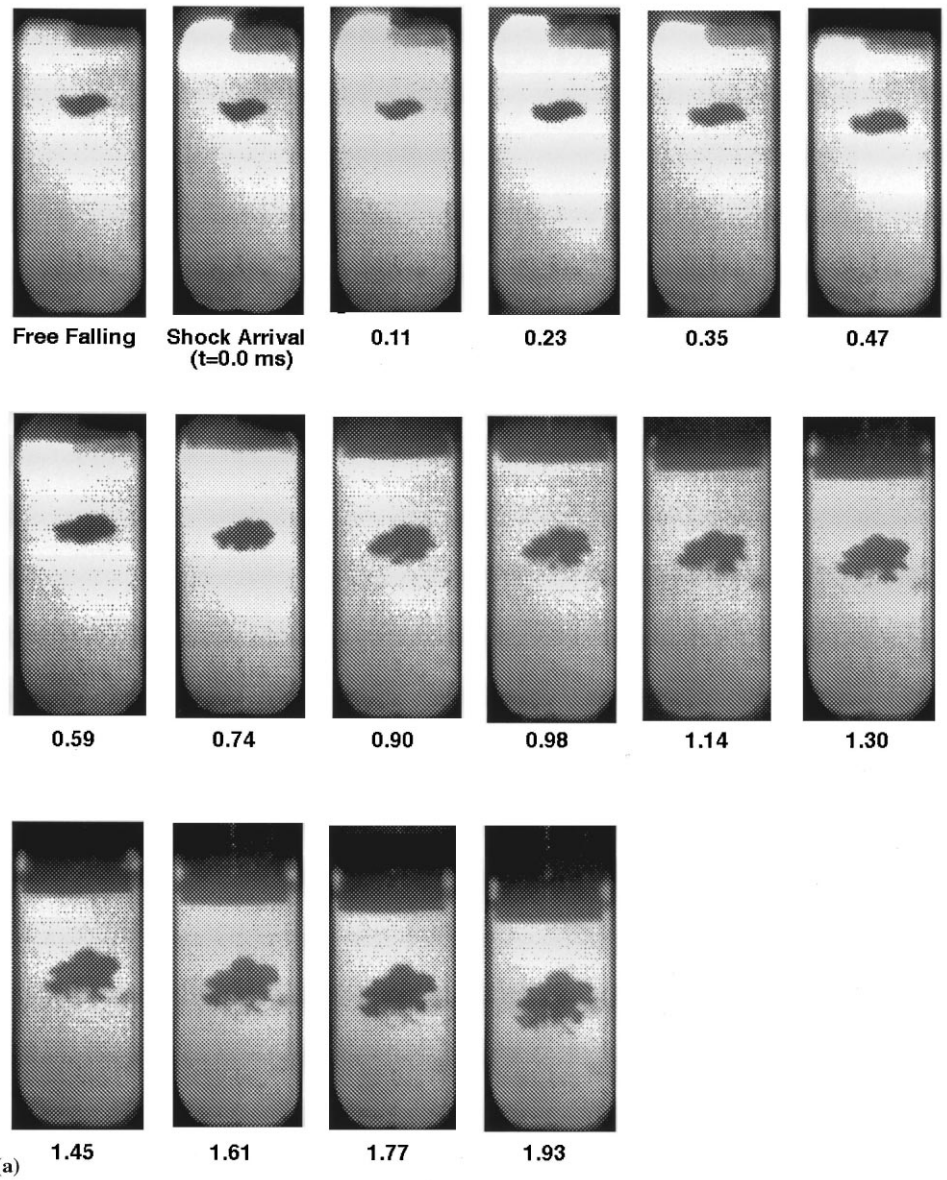

Fig. 4. Movie images of run G/240/45; (b) movie images of run T/204/1000; (c) movie images of run T/204/1800.

which in turn surrounds any remaining (coherent) drop mass. These data are complementary to those in the X-ray in the following sense. From the X-ray film we can distinguish the fragmented debris mass (as described shortly below); we can thus determine the amount of water mixed with the debris. The movies allow us to expand this information, from the selected time instances of the X-rays, to the complete explosion event.

Analysis of both the movie and X-ray images are done with a digital scanner (UMAX UC840), and associated software to compute local masses and total volumes. The manner in which the mass corresponding to the debris was identified is described in conjunction with the presentation of data in the next section.

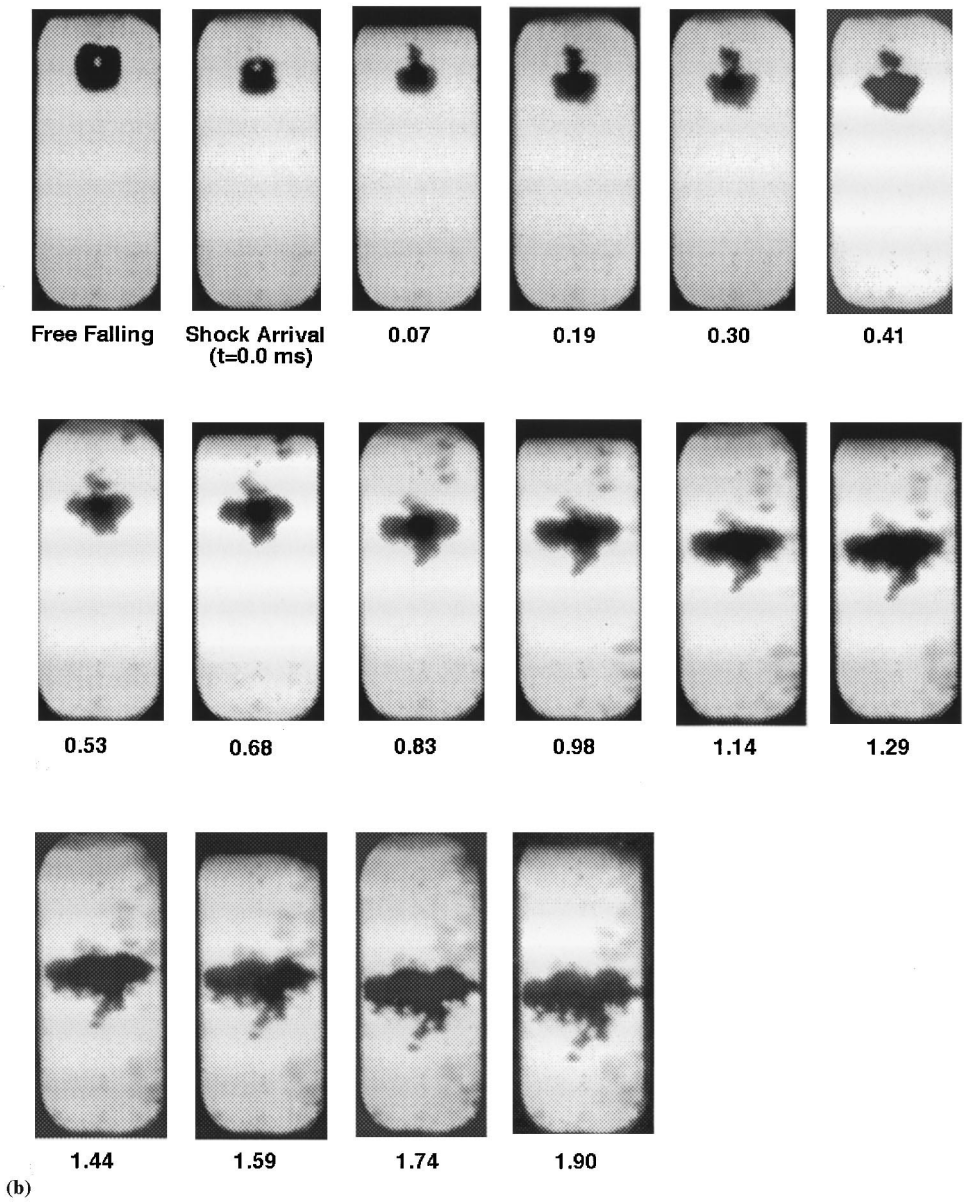

Fig. 4. (*Continued*)

The debris collected from the 'catcher' was washed, dried and subjected to sieve analysis. Selected samples were examined under the electron microscope.

The experimental program involved two melts and runs under seven conditions, as summarized in Table 1. The run identifier code includes shock pressure and melt temperature for easy identification in the discussion. Key properties of these melts are given in Table 2. Referring to a remark made in the introduction about iron, the properties of this material are also included. For the tin

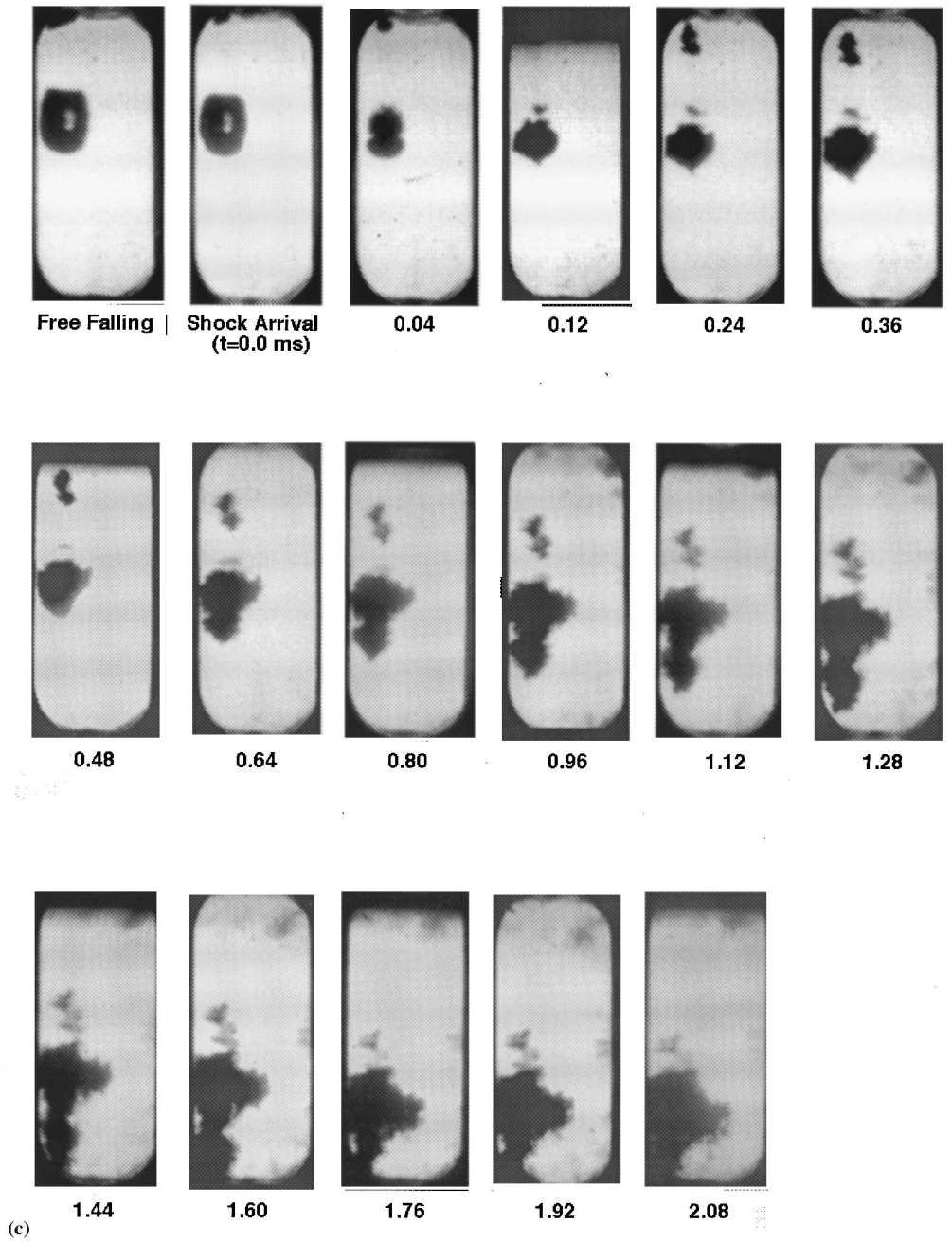

Fig. 4. (*Continued*)

runs, the water temperature was raised to 90°C, to prevent spontaneous interactions. In addition to one movie run for each entry in Table 1, we have three duplicate runs of T/204/1000 for the X-ray data at three selected instances (0.85, 1.0 and 1.5 ms).

4. Experimental results

Selected movie image sequences from three representative runs are shown in Fig. 4(a)–(c). It is interesting to note that in all cases, the boundary is highly structured, and that in the non-isothermal runs, the interaction zone develops in a highly irregular fashion. Note, however, that even for the high-temperature runs, the Microinteractions zone is quite confined around the drop, as found previously (Yuen et al., 1994). To obtain an indication of the volume of these zones, these images are integrated (using horizontal slices) assuming axial symmetry (for each slice separately). The uncertainty in carrying out the mechanics of this process is very low, so the real uncertainty depends on the assumption of axial symmetry which, strictly speaking, is not defined at this time. However, an overall perspective can be obtained from the time-wise regularity of the results as well as from the trends between various runs. All the volume results are presented together with analytical interpretations in Section 6.

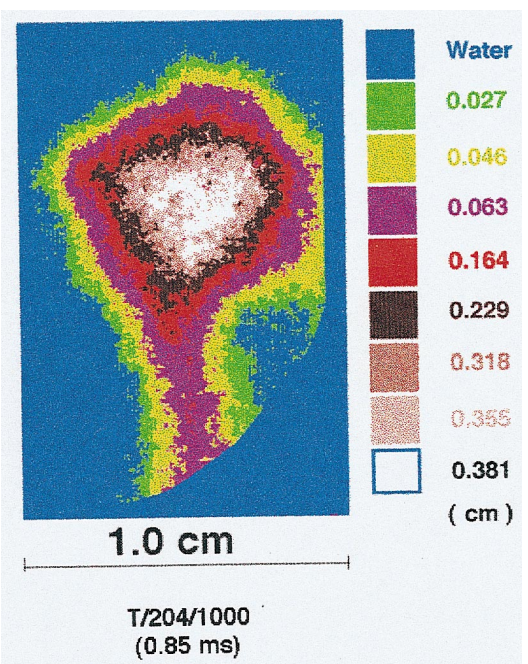

Fig. 5. Flash X-ray image of a tin drop (1000°C) at 0.85 ms after the shock arrival for run T/204/1000.

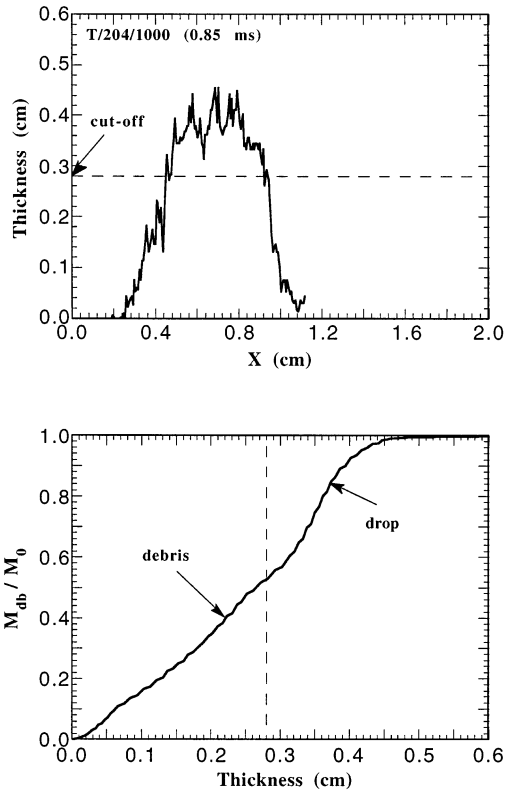

Fig. 6. Mass distribution results from the X-ray film shown in Fig. 5. The figure on the top represents the mass thickness distribution along the horizontal line containing the local area with the highest mass concentration. The figure on the bottom shows the cumulative mass fraction distribution.

A reconstructed X-ray image is shown in Fig. 5, and the mass thickness distribution along a horizontal axis going through the image at an elevation containing the point of maximum mass thickness is given at the top of Fig. 6. The sudden drop-off in thickness seen in this figure was used to identify a 'boundary' between the still-coherent drop mass and the surrounding debris. This, then, in conjunction with the cumulative mass distribution shown at the bottom of Fig. 6, was used to determine the fraction of the drop fragmented at the time the shot was taken. For the estimated drop mass, the equivalent diameter is 0.44 cm where the horizontal width of the cutoff thickness region is 0.49 cm and the 'average' thickness in

this region can be read as about 0.4 cm, a consistency which is indicative that the inner region identified as 'unfragmented' drop indeed contains no water. The reduced data from all three X-ray runs are presented together with analytical interpretation in Section 6.

The debris size distribution from all tin runs is summarized in Fig. 7. We note that the 'low pressure,' 'high temperature' combination gave the maximum fragmentation, while the 'low pressure,' 'low temperature' case produced essentially no fragmentation. The 'low' and 'high' characterization applied here are in the perspective of this work. In general, 1000°C is not really low, since researchers have worked extensively with tin at temperatures below 1000°C, and in the KROTOS experiments, tin melts at 1000°C were used in attempts to obtain propagating explosions. The present results explain why this was not possible (Yuen et al., 1994).

The debris structure can be seen from representative scanning electron microscope (SEM) photographs collected in Fig. 8. The small sample shown for each run was obtained to include particles from those in the fine powder range, to intermediate and large particle sizes. It is interesting to note the highly convoluted morphology of the large particles, even those at low temperatures, and the smooth shape of the fine particles in the high-temperature cases (those are absent in the low-temperature runs).

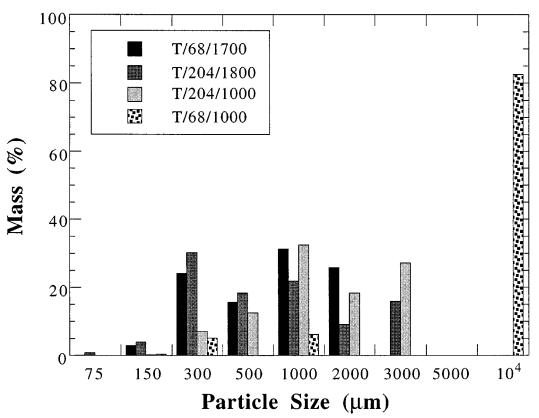

Fig. 7. Histogram of fragmented masses from the tin runs. (Data are shown on a pass-basis; i.e. the mass fraction shown at each sieve size corresponds to masses caught between it and the next higher size.)

5. The Microinteractions model in ESPROSE.m

As noted already, we wish to interpret the data presented above in the ESPROSE.m frame. This is done in the next section, by means of ESPROSE.m calculations. In this section, by way of introduction, we provide the key aspects of the model (Yuen and Theofanous, 1995).

In the multifield formulation of ESPROSE.m, the materials involved in the Microinteractions zone (called the m-fluid) are considered together as a separate field, that is allowed to interact with the other two fields (fuel and liquid coolant) through exchanges of mass, momentum and energy. For our present purposes, we are mainly interested in the continuity equations which are written, for the fuel (f), liquid coolant (l), the Microinteractions 'field' (m) and the debris (db), as follows:

$$\frac{\partial \rho'_{\mathrm{m}}}{\partial t} + \nabla \cdot (\rho'_{\mathrm{m}} \boldsymbol{u}_{\mathrm{m}}) = E + J \tag{1}$$

$$\frac{\partial \rho'_{\mathrm{l}}}{\partial t} + \nabla \cdot (\rho'_{\mathrm{l}} \boldsymbol{u}_{\mathrm{l}}) = -E - J \tag{2}$$

$$\frac{\partial \rho'_{\mathrm{f}}}{\partial t} + \nabla \cdot (\rho'_{\mathrm{f}} \boldsymbol{u}_{\mathrm{f}}) = -F_{\mathrm{r}} \tag{3}$$

$$\frac{\partial \rho'_{\mathrm{db}}}{\partial t} + \nabla \cdot (\rho'_{\mathrm{db}} \boldsymbol{u}_{\mathrm{m}}) = F_{\mathrm{r}} \tag{4}$$

In these equations, the 'source terms' F_{r} and E represent the rate of fuel fragmentation and the rate of entrainment of liquid coolant into the Microinteractions zone, respectively. These are the terms that need to be defined before the system of equations (including momentum and energy conservation which are not presented in detail here) can be integrated, and these are the constitutive laws under investigation here. The other source term J represents mass transfer by phase change between liquid coolant and m-fluid. In addition to Eqs. (1)–(4), we have an equation to keep track of the changes in the fuel length scale, written as:

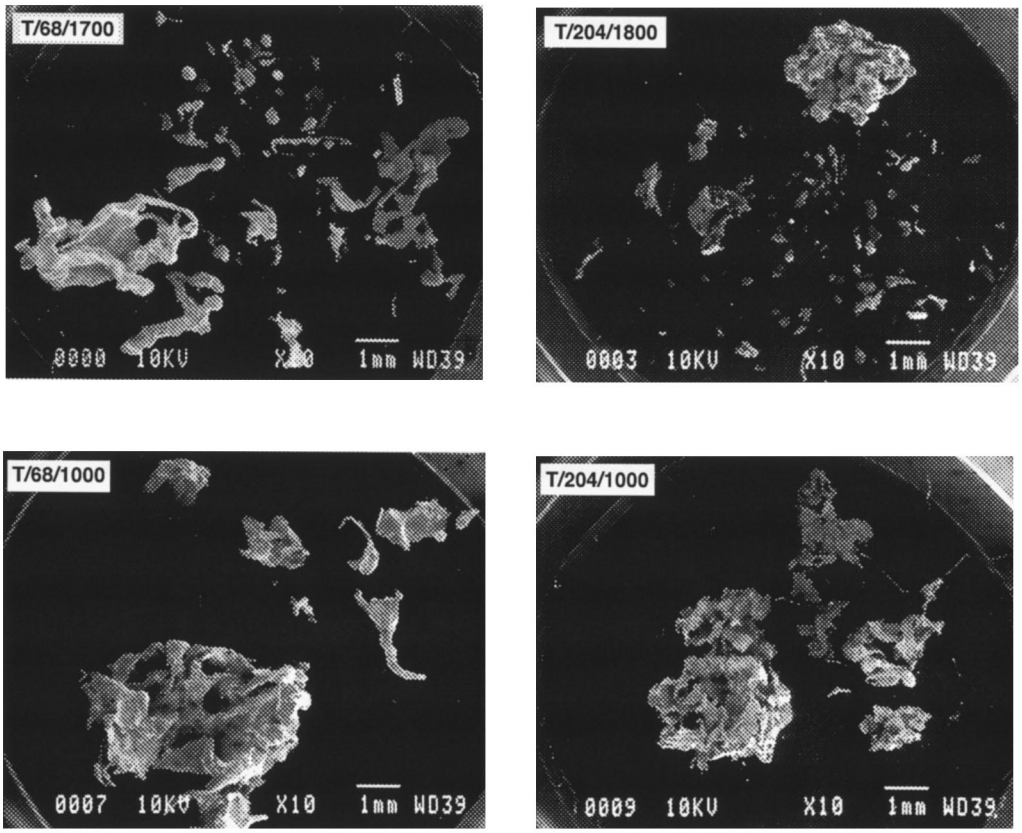

Fig. 8. SEM photographs of sample debris collected from four tin experiments (in each photograph samples of 'large,' 'medium' and 'small' debris are presented, to illustrate typical characteristic dimensions).

$$\frac{\partial}{\partial t}\left(\frac{\theta_f}{D_f}\right)+\nabla\cdot\left(\frac{\theta_f}{D_f}\boldsymbol{u}_f\right)=\frac{2\theta_f}{D_f^2}\frac{dD_f}{dt} \tag{5}$$

This equation is based on interfacial area transport considerations and includes a 'sink' term on the right hand side, representing the length scale changes due to fragmentation (the dD_f/dt term is related to the rate of fragmentation).

The hypothesis made in the original formulation of ESPROSE.m was that the entrainment rate is proportional to the rate of fragmentation (on a volume basis); that is,

$$E=f_e F_r\frac{\rho_l}{\rho_f} \tag{6}$$

where f_e is the 'entrainment factor.' The instantaneous fragmentation rate, F_r, is obtained from a characteristic fragmentation time, t_f, as:

$$F_r=\frac{\rho'_f}{t_f} \tag{7}$$

and the rate of change of the fuel particle diameter is given by

$$\frac{dD_f}{dt}=-\frac{D_f}{3t_f} \tag{8}$$

where the fragmentation time is estimated on the basis of an instantaneous Bond number formulation (i.e. based on the instantaneous differential velocity and drop diameter) obtained by extending an earlier formulation (Patel and Theofanous, 1981) to a high transient regime (Yuen et al., 1994); that is

$$t_f^*\equiv\frac{|\boldsymbol{u}_f-\boldsymbol{u}|t_f}{D_f}\epsilon^{-1/2}=\beta_f \mathrm{Bo}^{-1/4} \tag{9}$$

with

$$\mathrm{Bo} \equiv \frac{3C_d \rho D_f |\boldsymbol{u}_f - \boldsymbol{u}|^2}{16\sigma} \epsilon = \frac{\rho_f}{\rho_l} \tag{10}$$

This is for the purely hydrodynamic regime and β_f is evaluated in conjunction with the relevant experiments. For example, based on data available at the time, Yuen et al. (1994) found $\beta_f = 13.7$, while Theofanous et al. (1979) used $\beta_f = 10.3$. To represent rates of fragmentation higher than this value, due to thermal effect for example, we introduce an augmentation factor which, to a first approximation, is treated (here) as a constant; i.e. more generally, we have

$$t'_f = \frac{t_f}{\gamma_t} \tag{11}$$

and expect that $\gamma_t \to 1$ at very high pressures, where thermal effect can be expected to be negligible.

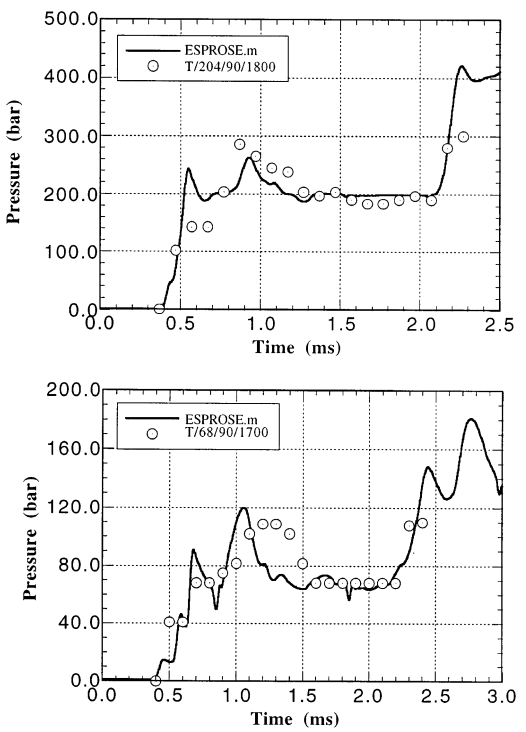

Fig. 9. Comparison between ESPROSE.m predictions and measurements of pressure at the transducer below the observation window for runs T/68/1700 and T/204/1800.

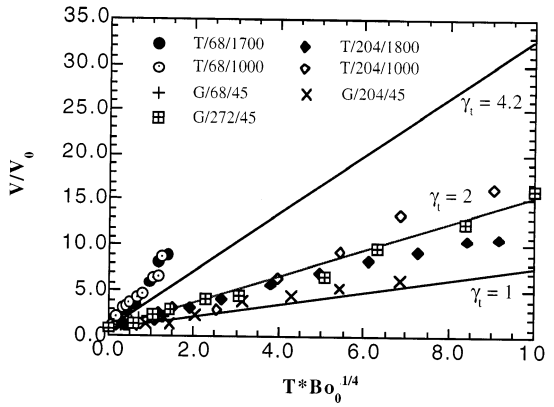

Fig. 10. Transient behavior of the mixing volume for the seven tests.

To recognize that by the time there is sufficient fragmentation, the turbulence developed and associated mixing effects cannot be expected to subside, even if the fragmentation rate diminishes (because of fuel depletion and/or approaching velocity equilibration), the entrainment rate in ESPROSE.m is kept as a non-decreasing function of time, i.e. it maintains its last maximum value.

The SIGMA simulations presented in the next section were carried out in one dimension with the melt drop at the appropriate location, and with a grid size of 1.25 cm to capture the highly localized event of interest. A small gas pocket in the melt generator was also simulated. The effect on the wave dynamics is to create an overshoot at the front end of the pressure pulse (this is absent in the absence of this gas pocket), which is both interesting and predictable, as seen in Fig. 9.

6. Data interpretations and discussion

Before the detailed interpretations with ESPROSE.m, it is instructive to consider the data in the interpretation of Patel and Theofanous (1981) and Yuen et al. (1994), that suggested a linear relation between the debris mass and dimensionless breakup time, i.e.:

$$\frac{M_{db}}{M_0} = \frac{1}{\beta_{f0}} \mathrm{Bo}_0^{1/4} \tag{12}$$

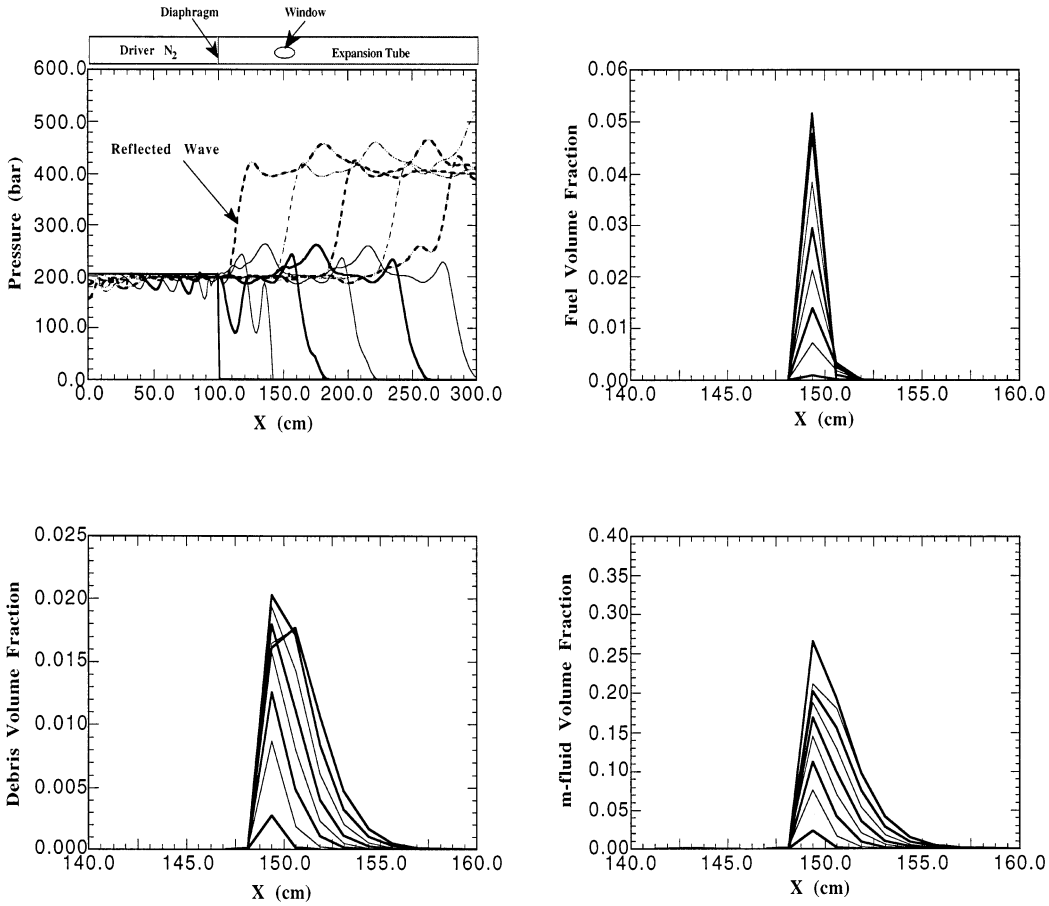

Fig. 11. A typical set of pressures, volume fraction distributions for fuel, debris and m-fluid predicted by ESPROSE.m (run T/204/1000) at 0.25 ms intervals. (The debris and m-fluid volume fraction distributed begin at 0.5 ms.)

Now combining this with Eq. (6), we can obtain:

$$\frac{V}{V_0} = 1 + \frac{f_e}{\beta_{f0}} t^* \mathrm{Bo}_0^{1/4} \tag{13}$$

where V includes the unfragmented drop mass and the water entrained into the Microinteractions zone. It is important to note that in Eq. (12), β_{f0} represents the total dimensionless fragmentation time based on the 'initial' Bond number. It should thus correspond approximately to β_f/γ_t for the fragmentation model described in the previous section. Eq. (13) is an approximation, since it is derived assuming a constant density for the entrained liquid (i.e. isothermal fragmentation).

All the high-speed movie data, plotted in the form suggested by Eq. (13), are shown in Fig. 10. This figure also contains the line of Eq. (13) with the values $f_e = 7$ and $\beta_f = 9$ and $\gamma = 1$, 2 and 4.2. The specific values of these parameters are determined from interpretation of the fragmentation data with ESPROSE.m, which is described below. A distinctive trend of the data can clearly be identified. As pressure increased, the fragmentation behavior approached the 'hydrodynamic regime' as represented by the isothermal gallium runs. The effect of temperature appears to be rather secondary.

A representative set of pressure transients, and volume fraction distributions of fuel, debris and

m-fluid obtained from ESPROSE.m with given values of the three constants (β_f, f_e and γ_t), are shown in Fig. 11. The following approach was used in this parameter identification exercise, using such numerical experiments.

First, we re-examine the old X-ray mercury fragmentation data (Yuen et al., 1994) to determine the value of β_f in the ESPROSE.m formulation that produces the same rates of fragmentation. The results are shown in Fig. 12. As expected, the entrainment f_e has essentially no effect on the predicted fragmentation. Based on this comparison, the value of β_f is determined to be 9. The value of 13.7 quoted by Yuen et al. (1994) was based on a very early version of the ESPROSE code and an approximate treatment of the instantaneous Bond number formulation. On the other hand, the value of β_f is actually quite close to the 10.3 value of Theofanous et al. (1979) noted above.

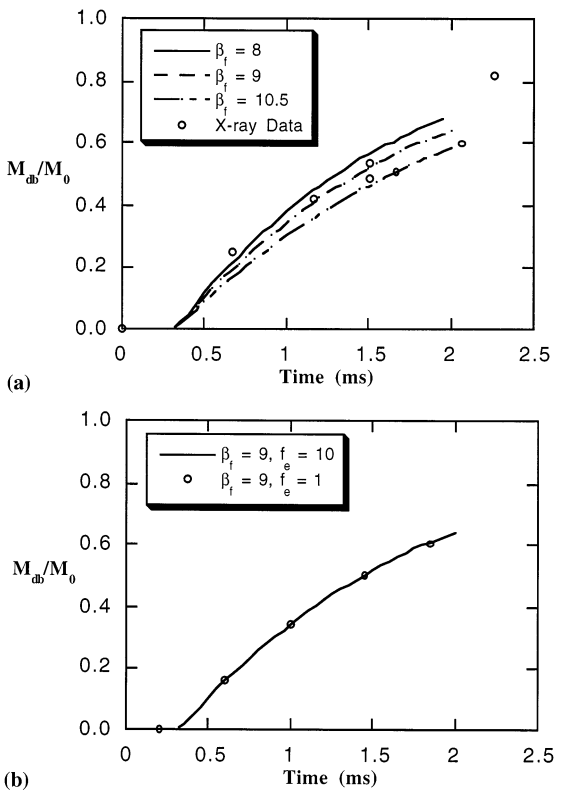

Fig. 12. Comparison between ESPROSE.m predictions and the old fragmentation data for mercury at 340 bar. The top figure shows the effect of β_f with $f_e = 10$. The bottom figure shows the effect of f_e with $\beta_f = 9$.

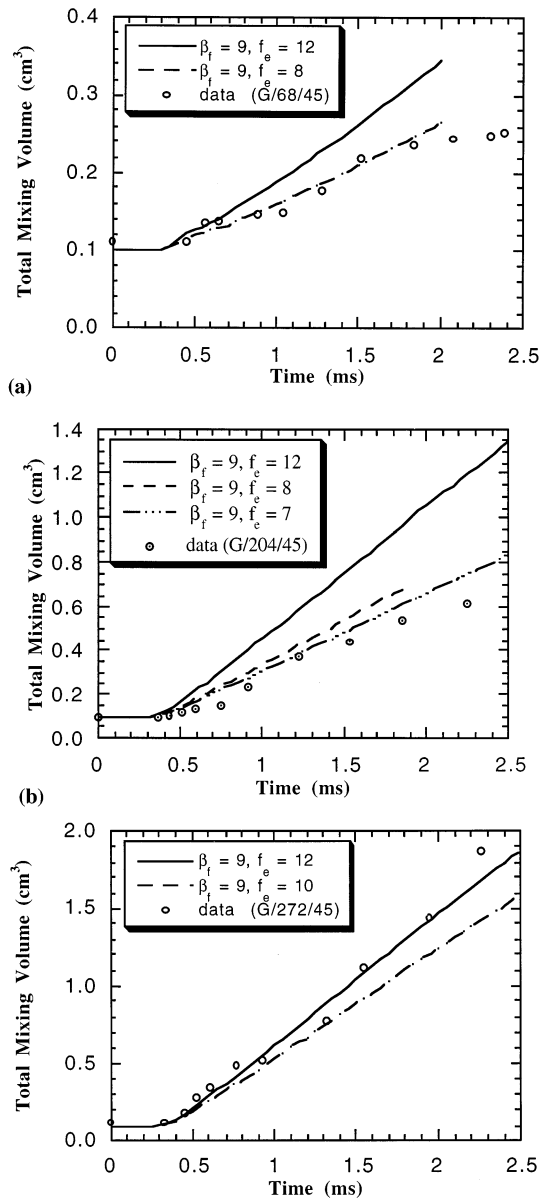

Fig. 13. Comparison between the predicted and measured mixing volumes for the isothermal gallium/water runs. Time zero corresponds to the moment of diaphragm rupture.

With the β_f fixed, numerical experiments are next run to determine an appropriate value of f_e

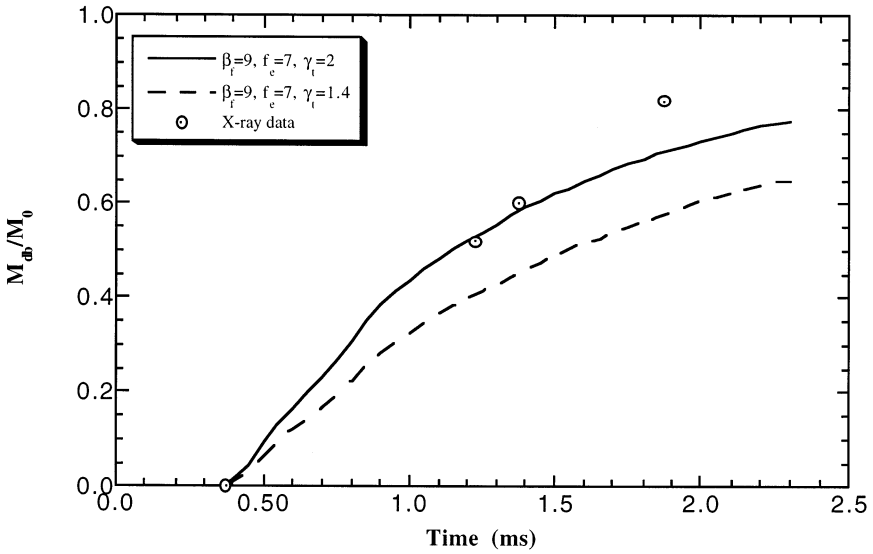

Fig. 14. Comparison between the ESPROSE.m prediction ($\beta_f = 9$, $\gamma_t = 2$) with the fragmentation data for the present X-ray tin runs (T/204/1000). Time zero corresponds to the time of the diaphragm rupture.

using comparisons of predicted and measured total volume (volume of the drop, debris and entrained coolant) with the three gallium runs. As shown in Fig. 13, there is some explicit dependence on pressure. However, the general trends are reasonable, in the perspective of the highly coupled nature of the phenomenon and of the data being analyzed here, and allow us to make a first-order choice of this parameter, f_e in the range 7–10. From the model described in Section 5, one can recognize that higher values lead to lower peak explosion pressure, so a value of 7 can be considered as reasonably conservative for highly developed detonations. This is the value used in sample calculations with ESPROSE.m so far (Yuen and Theofanous, 1994; Theofanous and Yuen, 1994).

Next, the X-ray tin data are examined with the values of β_f and f_e fixed at 9 and 7, respectively. We find that some augmentation of the fragmentation rate is required. With a value of $\gamma_t = 2$, the comparison of the data is reasonable, as shown in Fig. 14. Also in Fig. 14, we can see that the sensitivity to γ_t is not great. The value of γ_t is in fact consistent with the movie data and the other high-pressure run (T/204/1800) as shown in Fig. 15. For the low-pressure runs, a much higher enhancement factor is necessary ($\gamma_t = 4.2$) to produce the agreement seen in Fig. 15. A summary of the Microinteractions parameters determined from the tin data is shown in Table 3.

7. Conclusions

The purpose of this paper is to present the first systematic evaluation of the Microinteractions model used in the ESPROSE.m code to compute the propagation phase of steam explosions. The approach is basically experimental, using the SIGMA-2000 facility to observe exploding tin drops under conditions that simulate those found in large-scale, fully developed detonations. The results indicate that to a first approximation, the basic form of the constitutive laws hypothesized in the original formulation of ESPROSE.m is appropriate. Moreover, the results clearly show that under high-pressure conditions a hydrodynamic regime dominates the behavior. The data, in conjunction with numerical experiments, have made it possible to determine numerical constants in the formulation of the hydrodynamic regime,

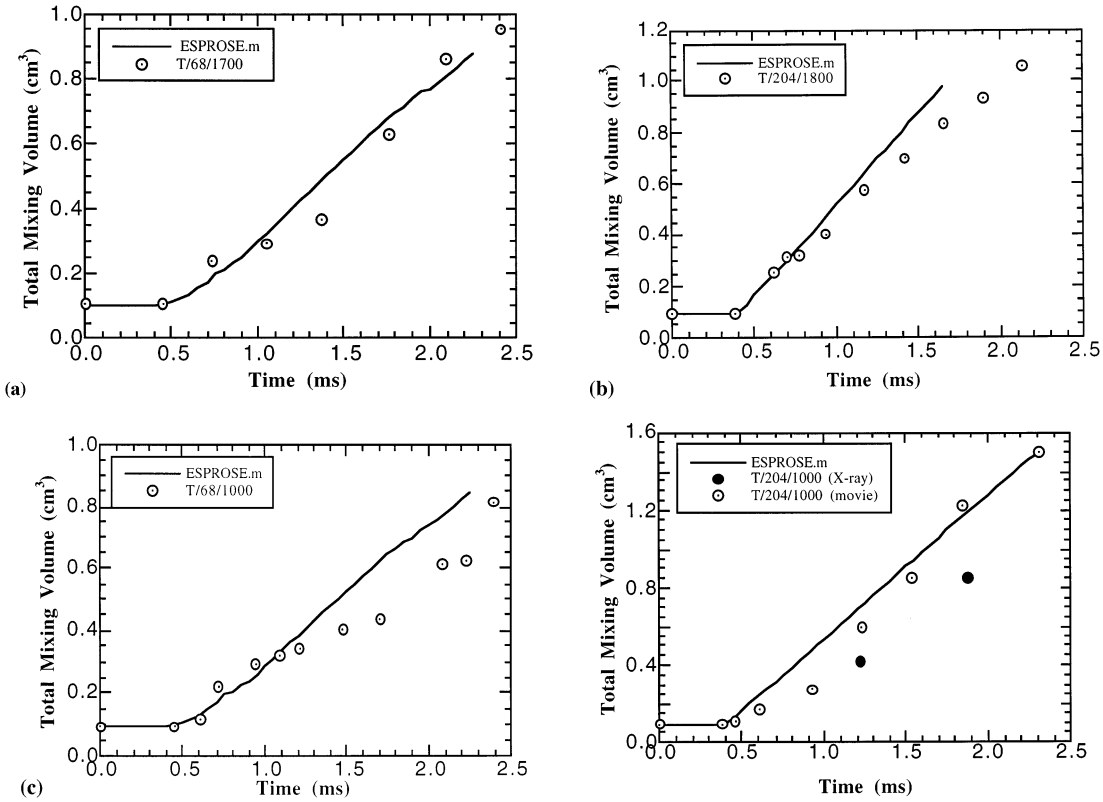

Fig. 15. Comparison between the predicted (with $\beta_f = 9$, $f_e = 7$) and measured mixing volumes for all present tin movie runs. Time zero corresponds to the time of diaphragm rupture. For run T/204/1000, the data points from the X-ray runs are also presented.

and to attempt a first quantification of the thermal regime.

8. Nomenclature

Bo Bond number, Eq. (10)
C_d drag coefficient
D drop diameter
E mass entrainment rate
f_e entrainment factor, Eq. (6)
F_r fragmentation rate
t time
t_f^* dimensionless complete fragmentation time of one fuel particle, Eq. (9)
$\boldsymbol{u}$ velocity vector

Greek letters
β_f fragmentation constant, Eq. (9)
γ_t thermal enhancement factor
ϵ density ratio, Eq. (10)
θ volume fraction
ρ microscopic density
ρ' macroscopic density, Eqs. (1)–(4)
σ surface tension

Subscripts
db debris
f fuel (also fragmentation)
l liquid
m m-fluid (m-field)

Table 3
Microinteraction model parameters deduced from the tin experiments

Run ID	Temperature (water/melt) (°C)	Pressure (bar)	β_f	f_e	γ_t
T/68/1700	90/1700	68	10.5	10	4.2
T/204/1800	90/1800	204	10.5	10	1.4
T/68/1000	90/1000	68	10.5	10	4.2
T/204/1000	90/1000	204	10.5	10	1.4

Acknowledgements

This work was funded by the US Department of Energy's Advanced Reactor Severe Accident Program (ARSAP) through ANL subcontract No. 23572401. We are grateful to Mr Steven Sorrell (DOE) and Mr Stephen Addition (TENERA) for their key roles in programmatically supporting this program.

References

Fletcher, D.F., Anderson, R.P., 1990. A review of pressure induced propagation models of the vapor explosion process. Progr. Nucl. Energy 23, 137–179.

Patel, P.D., Theofanous, T.G., 1981. Hydrodynamic fragmentation of drops. J. Fluid Mech. 103, 207–223.

Theofanous, T.G., Saito, M., Ethimiadis, T., 1979. The role of hydrodynamic fragmentation in fuel–coolant interactions. 4th CSNI Specialist Meet. Fuel–Coolant Interactions in Nuclear Reactor Safety, Bournemouth, England, Apr. 2–5, 1979. CSNI Report No. 37, vol. 1, 112, Paper # FC 14/P5.

Theofanous, T.G., Yuen, W.W., 1994. The prediction of dynamic loads from ex-vessel steam explosion. Proc. Int. Conf. New Trends in Nuclear System Thermohydraulics, Pisa, Italy, vol. 2, pp. 257–270.

Yuen, W.W., Chen, X., Theofanous, T.G., 1994. On the fundamental microinteractions that support the propagation of steam explosion. Nucl. Eng. Des. 146, 133–146.

Yuen, W.W., Theofanous, T.G., 1994. The prediction of 2D thermal detonations and resulting damage potential. Proc. CSNI Specialists Meet. Fuel–Coolant Interaction, NUREG/CP 0127, Mar. 1994, pp. 233–250.

Yuen, W.W., Theofanous, T.G., 1995. ESPROSE.m: a computer code for addressing the escalation/propagation of steam explosions, DOE/ID-10501.

.